Laser frequency stabilization with toroidal optical microresonators

M. McGovern[a], T.G. McRae[a], G. Turner[b], A. J. Kay[c], R. J. Blaikie[b], and W. P. Bowen[a]

[a]Jack Dodd Centre for Photonics and Ultracold Atoms, Department of Physics, University of Otago, Dunedin, New Zealand;

[b]Department of Electrical and Computer Engineering, University of Canterbury, Christchurch, New Zealand

[c]Opto-organics group, Industrial Research Limited, P.O. Box 31 310 Lower Hutt, New Zealand

ABSTRACT

Progress towards semiconductor laser frequency stabilization using optical feedback from microtoroidal resonators is presented. A simple model of the feedback mechanism is provided, and equations of motion describing the system fields are given. Reactive ion etcher based fabrication of microtoroidal resonators with intrinsic quality factors as high as 1.6×10^5 is demonstrated. This fabrication technique enables improved silicon surface quality and greater control of the physical structure of the microresonators.

Keywords: Reactive ion etch, microfabrication, microtoroid, microresonator, frequency stabilization, optical clocks, whispering-gallery mode

1. INTRODUCTION

Optical resonators are an integral component of almost all photonic systems, and have numerous applications in communications, spectroscopy, nonlinear optics, and laser physics.[1] Their usefulness arises from their ability to confine light both spatially and temporally. The temporal confinement is quantified by the resonator quality Q, and the spatial confinement by the optical mode volume V. Many applications of optical resonators require high intra-resonator field intensities, or in other words strong confinement both temporally (high Q), and spatially (low V). As a result, the last two decades have seen a strong push to achieve resonators with increasingly large Q and small V.[1]

In present systems Fabry-Perot resonators, where light resonates between a pair of dielectric mirrors, are predominantly used. However, such resonators have serious limitations, both in terms of optical confinement, and integration into existing systems. Whispering gallery mode (WGM) resonators, where light is confined by glancing incidence reflection off the inner surface of a dielectric medium, offer the potential to overcome both of these limitations. Unprecedented Q and V have recently been achieved through the development of ultrahigh Q microtoroidal WGM resonators.[2] These microtoroids are silicon chip based and fiber coupled, and are hence well suited to photonics applications and microresonator research.[3–7]

In this paper, we investigate frequency stabilization of semiconductor lasers using microtoroids. Lasers exhibiting high frequency stability are essential to many areas of science including optical atomic clocks,[8,9] and quantum information science.[10] Over the past decade impressive sub-Hz stability levels have been achieved with semiconductor lasers actively locked to vibration isolated Fabry-Perot resonators.[11] However, the complex nature of such state-of-the-art systems is prohibitive to widespread use. Microtoroids offer the potential for compact, robust, integrated laser frequency stabilization of broad utility to research laboratories and industry, albeit at kHz rather than Hz stability levels.

We report progress towards semiconductor laser frequency stabilization with microtoroids. A basic model of the feedback mechanism in these systems is presented, which allows a qualitative understanding of the ideal coupling parameters. To obtain a more quantitative understanding a set of non-linear equations of motion

Further author information: (Send correspondence to W.P.B.)
W.P.B.: E-mail: wbowen@physics.otago.ac.nz, Telephone: 64 3 479 7754

Photonics: Design, Technology, and Packaging III
edited by Wieslaw Z. Krolikowski, Costas M. Soukoulis, Ping Koy Lam, Timothy J. Davis, Shanhui Fan, Yuri S. Kivshar
Proc. of SPIE Vol. 6801, 68010Y, (2008) · 0277-786X/08/$18 · doi: 10.1117/12.769329

Downloaded From: http://proceedings.spiedigitallibrary.org/ on 11/18/2015 Terms of Use: http://spiedigitallibrary.org/ss/TermsOfUse.aspx

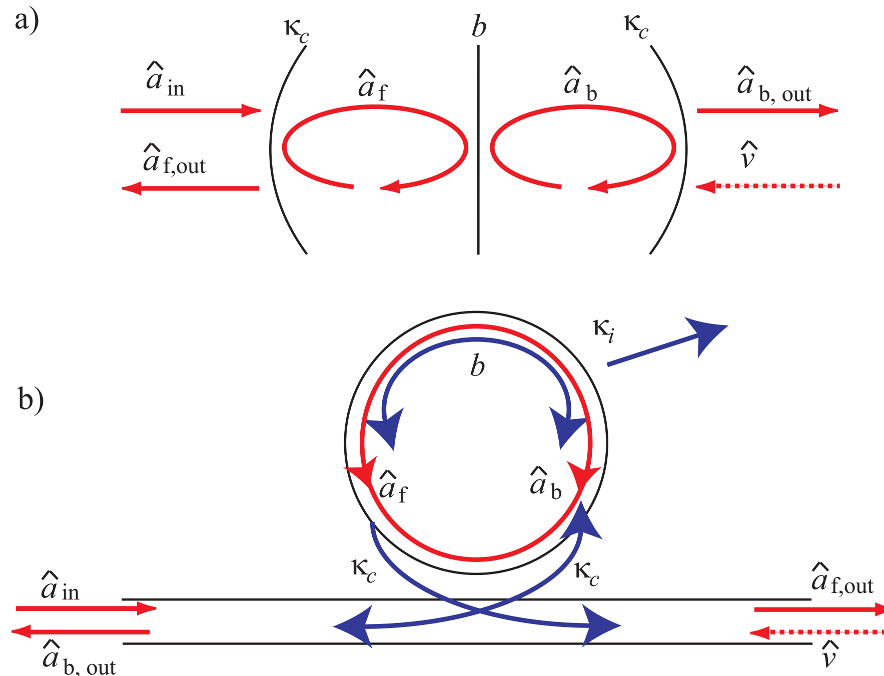

Figure 1. Model of a microtoroid coupled to a tapered optical fiber. a) Fabry-Perot resonator equivalent model b) fiber/microtoroid model.

must be solved. Extending the work of Kitching *et al.*,[12] Agrawal,[13] and Oraevskii *et al.*[14] we identify the appropriate equations, the solution of which will be presented in a separate publication.[15] Further, we report the development of a microtoroid fabrication technique based on reactive ion etching. When compared to standard xenon difluoride etching techniques our technique offers substantially improved silicon surface quality and the capability to perform anisotropic etching and hence greater control of the final microtoroid physical structure. Intrinsic quality factors as high as 1.6×10^5 have been observed, limited primarily by contamination during the reactive ion etching process.

2. COUPLED RESONANCES IN MICROTOROIDS

The effects of external cavities coupled to semiconductor lasers has been relatively well documented.[16–20] In particular, the use of optical feedback (OFB) can effectively narrow the linewidth of a semiconductor laser, and lock its frequency to the resonant frequency of the external cavity. To date, semiconductor lasers with linewidth narrowing of over 10 orders of magnitude[21] have been demonstrated using a system of Fabry-Perot external cavities, as well as servo electronics to control both the mechanical and thermal vibrations. Such systems however are large, sophisticated and complex, which limits their widespread utility.

This paper investigates semiconductor laser frequency stabilization with a new form of optical cavity, the toroidal microresonator. These microtoroids are microfabricated, scalable, fiber coupled devices, and offer the potential for significant improvements over existing technologies in terms of robustness and widespread applicability. Microtoroids confine light via total internal reflection in whispering-gallery modes (WGM), and can be optically excited using the evanescent wave from a coupling device such as a tapered optical fiber[22] as shown in Fig. 1 b). For the orientation shown in the figure, the tapered fiber excites counter-clockwise propagating field modes. Rayleigh backscattering of these fields in turn excites clockwise propagating fields with a characteristic rate b, resulting in a two-contour coupled resonance system. The excitation in the resonator decays with a characteristic rate $\kappa = \kappa_i + \kappa_c$ where κ_i is the intrinsic loss rate attributed to optical scattering, absorption, and

Downloaded From: http://proceedings.spiedigitallibrary.org/ on 11/18/2015 Terms of Use: http://spiedigitallibrary.org/ss/TermsOfUse.aspx

bending losses, and κ_c is the input coupling rate from the taper. These loss rates can be linked to the quality factor of the cavity Q via the expression

$$Q = \frac{\omega}{\Delta\omega} = \frac{\omega}{2\kappa}, \tag{1}$$

where $Q^{-1} = Q_i^{-1} + Q_c^{-1}$ with Q_i being the intrinsic Q of the resonator, and Q_c the contribution to Q due to coupling.

Fig. 1 a) shows a simple model of the field interactions in a microtoroid. From this model, we obtain the equations of motion

$$\dot{\hat{a}}_{\rm f} = -\hat{a}_{\rm f}(\kappa + \imath\Delta) - \imath b\hat{a}_{\rm b} - \sqrt{2\kappa_c}\hat{a}_{\rm in}(t) \tag{2}$$

$$\dot{\hat{a}}_{\rm b} = -\hat{a}_{\rm b}(\kappa + \imath\Delta) - \imath b\hat{a}_{\rm f} - \sqrt{2\kappa_c}\hat{v}(t), \tag{3}$$

where $\hat{a}_{\rm b}$ and $\hat{a}_{\rm f}$ are slowly varying Heisenberg annihilation operators describing the clockwise and counter-clockwise cavity fields; $\hat{a}_{\rm in}(t)$ and $\hat{v}(t)$ are annihilation operators describing the input field and vacuum input, respectively; $\Delta = \omega_{\rm rot} - \omega_{\rm cavity}$ is the cavity detuning, where $\omega_{\rm cavity}$ is the resonant cavity frequency and $\omega_{\rm rot}$ is the rotating frame frequency; and b is the backscattering rate between anticlockwise and clockwise propagating modes. As usual, all annihilation operators have the properties $[\hat{a}^\dagger, \hat{a}] = 1$, and $\hat{a} = \alpha + \delta\hat{a}$, where $\alpha = \langle\hat{a}\rangle$ is the coherent amplitude and $|\alpha|^2$ the mean number of photons of the field.

Here, we are predominantly interested in the spectral response function of the fiber-coupled microtoroid system. Taking the Fourier transform of the expectation values of Eqs. (2) and (3), we obtain

$$\imath\omega'\alpha_{\rm f}(\omega') = -\alpha_{\rm f}(\omega')(\kappa + \imath\Delta) - \imath b\alpha_{\rm b}(\omega') - \sqrt{2\kappa_c}\alpha_{\rm in}(\omega') \tag{4}$$

$$\imath\omega'\alpha_{\rm b}(\omega') = -\alpha_{\rm b}(\omega')(\kappa + \imath\Delta) - \imath b\alpha_{\rm f}(\omega'), \tag{5}$$

which can be easily solved to give

$$\alpha_{\rm f}(\omega') = \frac{-\sqrt{2\kappa_c}\alpha_{\rm in}Z}{Z^2 + b^2}, \tag{6}$$

and

$$\alpha_{\rm b}(\omega') = \frac{\sqrt{2\kappa_c}\alpha_{\rm in}g}{Z^2 + b^2}, \tag{7}$$

for the intracavity coherent amplitudes, where $Z = \kappa + \imath(\omega' + \Delta)$ and ω' is a sideband frequency such that $\omega = \omega_{\rm rot} + \omega'$. The intracavity fields can be related to the forwards $\alpha_{\rm out,f}(\omega')$ and backwards $\alpha_{\rm out,b}(\omega')$ propagating fields in the tapered fiber using the input/output relations[23]

$$\alpha_{\rm out,f}(\omega') = \sqrt{2\kappa_c}\alpha_{\rm f} + \alpha_{\rm in} \tag{8}$$

$$\alpha_{\rm out,b}(\omega') = \sqrt{2\kappa_c}\alpha_{\rm b}. \tag{9}$$

It is then straightforward to determine the spectral response of the forward-going transmission T and backward-going feedback F

$$T(\omega') = \frac{|\alpha_{\rm out,f}|^2}{\alpha_{\rm in}^2} = \left[1 - \frac{2\kappa_c Z}{Z^2 + b^2} - \frac{2\kappa_c Z^*}{Z^{*2} + b^2} + \frac{4\kappa_c^2|Z|^2}{|Z^2 + b^2|^2}\right] \tag{10}$$

$$F(\omega') = \frac{|\alpha_{\rm out,b}|^2}{\alpha_{\rm in}^2} = \frac{4\kappa_c^2}{|Z^2 + b^2|^2}. \tag{11}$$

The transmission and feedback are plotted as a function of microtoroid input coupling rate κ_c in Fig. (2) a) and b), respectively. As expected, when the coupling rate is small ($\kappa_i \ll \kappa$) there is essentially no interaction between the taper and the microtoroid. This is the regime where the taper is far from the cavity and hence the transmission is unity. As the coupling rate increases the transmission decreases until it reaches zero at the critical coupling rate

$$\kappa_c^{\rm crit} = \sqrt{\kappa_i^2 + b^2}. \tag{12}$$

Downloaded From: http://proceedings.spiedigitallibrary.org/ on 11/18/2015 Terms of Use: http://spiedigitallibrary.org/ss/TermsOfUse.aspx

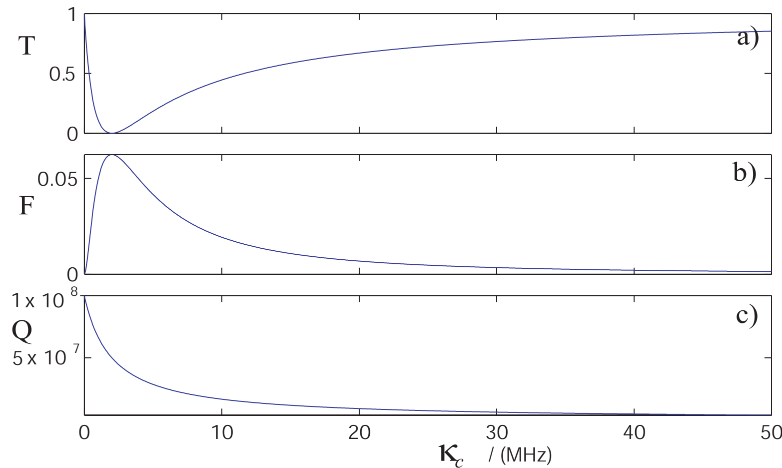

Figure 2. a) Transmission of the forward propagating field in the fiber as a function of κ_c. b) Feedback as a function of κ_c. c) Q as a function of κ_c. Parameters: $\kappa_i = 2$ MHz; b $= 0.1$ MHz; $\Delta = \omega' = 0$.

At even higher coupling rates the transmission increases back towards unity. Of course, the feedback F has the reverse behavior, with a peak at the critical coupling rate and a decline towards zero in both directions away from this point. The system is said to be undercoupled when $\kappa_c < \kappa_c^{\mathrm{crit}}$ and overcoupled when $\kappa_c > \kappa_c^{\mathrm{crit}}$.

Feedback ratios below $F \sim 10^{-4}$ are usually chosen in external cavity stabilized semiconductor lasers to avoid frequency and amplitude instabilities.[20] It can be seen from Fig. 2 b) that such small feedback ratios only occur in the far under- and over-coupled regimes. The line narrowing in frequency stabilized semiconductor lasers is proportional to the external cavity linewidth,[13] which is inversely proportional to Q (see Eq. (1)). Hence, as can be seen from Fig. (2) c), microtoroid based laser frequency stabilization should be performed in the far undercoupled regime.

3. LASER FREQUENCY STABILIZATION WITH MICROTOROIDS

Section 2 dealt primarily with the transmission and feedback spectral response functions of a microtoroid. However, to model the resulting semiconductor laser spectral line narrowing an analysis of the frequency noise of the combined laser/external resonator system must be undertaken. This sort of analysis has been performed for many external cavity based laser frequency stabilization systems.[13,18,19] However, as yet no such analysis has been performed for two-contour coupled resonance systems such as microtoroids. An intermediate model looking at the regimes of stability of semiconductor lasers coupled to two-contour coupled resonance cavities has been developed by Oraevskii *et al.*,[14] with experimental investigations on microsphere resonators by Vassiliev *et al.*.[24] However, this model does not include noise terms, and hence does not allow for the investigation line-narrowing.

Fig. 3 show the transmission spectral response function T of a microtoroid as a function of ω' for a range of backscattering rates b. At low scattering rates ($b \ll \kappa$) the spectral response function is a Lorentzian identical to that of a Fabry-Perot resonator; and at high scattering rates ($b \gg \kappa$) it consists of two such Lorentzians separated by $2b$. However, in the intermediate region shown in Fig. 3 b) the spectral response function is complex and not straightforwardly related to that of any system previously analyzed. To fully model laser line narrowing induced by external feedback from a microtoroid, a full dynamical analysis of the frequency noise properties of the combined system is therefore required.

The dynamical behavior of the coupled microtoroid/semiconductor laser system can be modeled by extending the rate equations given in[12] to the case where the external cavity is of the two-contour coupled resonance type.

Downloaded From: http://proceedings.spiedigitallibrary.org/ on 11/18/2015 Terms of Use: http://spiedigitallibrary.org/ss/TermsOfUse.aspx

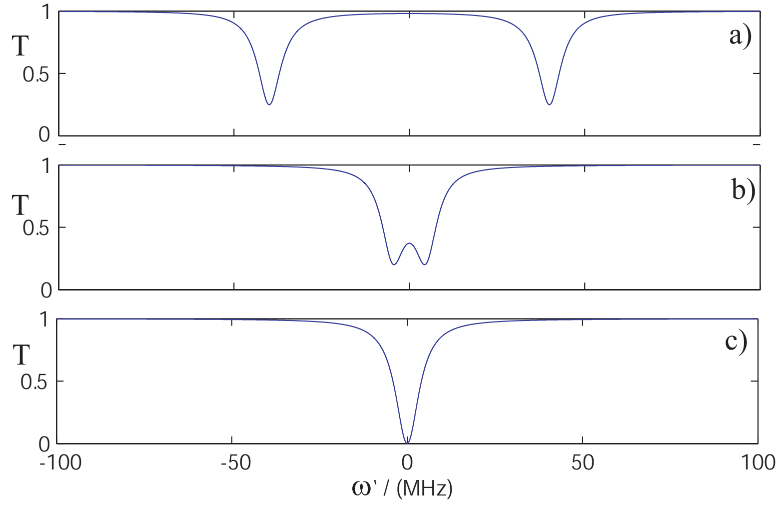

Figure 3. Transmission spectral response function as a function of ω' with varying backscattering rate. a) $b = 40$ MHz b) $b = 5$ MHz c) $b = 0.5$ MHz. Parameters: $\kappa_c = \kappa_i = 2$ MHz, $\Delta = 0$.

This yields the following set of equations

$$
\begin{aligned}
\frac{\mathrm{d}\hat{a}(t)}{\mathrm{d}t} &= -\frac{1}{2}\left[\frac{1}{\tau_p} + 2i\Delta_D - \frac{\omega}{\mu^2}(\hat{\chi}_i - i\hat{\chi}_r)\right]\hat{a} + \sqrt{2\kappa_c}\sqrt{2\kappa_d}\hat{a}_b(t-\tau)e^{i\omega_L\tau} \\
&+ \hat{G} + \hat{g} + \sqrt{2\kappa_d}\hat{v} \qquad (13) \\
\frac{\mathrm{d}\hat{a}_f(t)}{\mathrm{d}t} &= -\frac{1}{2}\left[\kappa_i + i2\Delta\right]\hat{a}_f - ib\hat{a}_b - \sqrt{2\kappa_c}\sqrt{2\kappa_d}\hat{a}(t-\tau)e^{i\omega_L\tau} \\
&- 2\kappa_c\hat{a}_b(t-2\tau)e^{i\omega_L 2\tau} - \hat{g}_c - \sqrt{2\kappa_c}\hat{v} \qquad (14) \\
\frac{\mathrm{d}\hat{a}_b(t)}{\mathrm{d}t} &= -\frac{1}{2}\left[\kappa_i + i2\Delta\right]\hat{a}_b - ib\hat{a}_f - \hat{g}_c - \sqrt{2\kappa_c}\hat{v}(t+\tau)e^{-i\omega_L\tau} \qquad (15) \\
\frac{\mathrm{d}\hat{N}_c(t)}{\mathrm{d}t} &= P - \frac{\hat{N}_c(t)}{\tau_{sp}} - \frac{\omega}{\mu^2}\hat{\chi}_i\hat{a}^\dagger\hat{a} - \left\langle \frac{\omega}{\mu^2}\hat{\chi}_i \right\rangle + \Gamma_p(t) + \Gamma_{sp}(t) + \Gamma(t), \qquad (16)
\end{aligned}
$$

where $\hat{a}$, and $\hat{N}_c$ are slowly varying Heisenberg annihilation operators for the internal diode field and the carrier population difference operator in the semiconductor, respectively, τ_p is the photon lifetime in the semiconductor material, Δ_D is the detuning of the laser carrier frequency ω_L from the resonant frequency of the internal diode cavity, μ is the nonresonant refractive index, $\hat{\chi}$ the resonant optical susceptibility operator, κ_d is the loss rate from the facet of the diode, τ is the optical distance (in s) from the diode facet to the external cavity, τ_{sp} is the semiconductor population difference decay time due to spontaneous emission, and P is the semiconductor pumping rate. The Langevin noise operators $\hat{G}$, $\hat{g}$, $\hat{g}_c$ and $\hat{v}$ are associated with dipole moment fluctuations, internal optical losses, external cavity optical losses, and incident vacuum fluctuations, respectively. Γ_p, Γ_{sp} and Γ correspond to pump noise, carrier noise that is due to spontaneous emission into nonlasing modes, and dipole moment fluctuations, with the correlation relations between noise terms given in.[12, 25] The solution to these equations is beyond the scope of this paper, and will be presented in a later publication.[15]

4. MICROTOROID FABRICATION

Fig. 4 shows a schematic of the microtoroid fabrication process which consists of wet etching to define a silica microdisk, dry etching to undercut this disk, and finally CO_2 laser reflow to smooth the rim of the disk. The dry

Downloaded From: http://proceedings.spiedigitallibrary.org/ on 11/18/2015 Terms of Use: http://spiedigitallibrary.org/ss/TermsOfUse.aspx

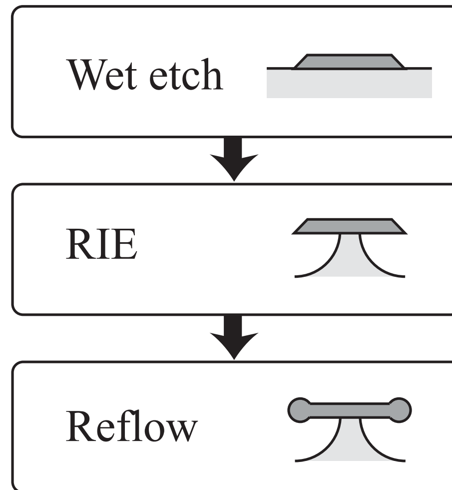

Figure 4. Schematic of the microtoroid fabrication process.

etching stage of microtoroid fabrication has traditionally been achieved with the use of XeF_2 in the vapor phase where the products of the etch, Xe and SiF_4, are also in the vapor phase and no plasma is required to produce the etching species.[26] This process etches the silicon with a selectivity to silica of 3000:1 and the isotropic nature of the etch allows the pedestal structure to be well separated from the rim of the microdisk. This isolation of the rim is important to isolate optical power that would otherwise leak into the silicon which has a higher refractive index.[2] The XeF_2 etch produces a granular structure on the etched silicon surface with features up to 10 μm and therefore this process is not suitable for applications where a polished surface is required. Such a surface is desirable, for example, for strong coupling in cavity quantum electrodynamics[7] where the reflective surface of the wafer could form an integral part of the magneto-optic trapping and cooling system. The isotropic nature of the etch also limits control over the pedestal dimensions. Additional control could be useful for the study of the radiation pressure induced coupling of mechanical and optical resonance in ultra high Q devices.[27] With these conditions in mind and motivated by the the work of Verbert *et. al.*[28] we replace the XeF_2 etch with an SF_6/O_2 reactive ion etch. Reactive ion etching processes allow both isotropic and anisotropic etching, and generally provides a much smoother silicon surface.

4.1. Wet Etch

The silicon wafers used in our studies were undoped with resistivities greater than 10 ohm-cm and an orientation of <100>. The 2 μm SiO_2 layer was grown on the silicon wafers by wet oxidation. This method of oxidation was chosen because the oxide is of much higher quality than the oxides deposited using the lower temperature chemical vapor deposition processes, as there are fewer hydroxide molecules that strongly absorb in the 1550 nm band.[2] The wafers were degreased and the surface was treated with HMDS to promote the adhesion of 1.5 μm of photoresist. The sample was then soft baked, exposed, developed and then hard baked to reflow the edges and smooth any lithographic blemishes and to improve physical and chemical stability to the subsequent buffered HF etch. The buffered HF etch was used to isotropically etch the SiO_2 and undercut the photoresist leaving a circular microdisk with a wedge shaped edge.

4.2. Reactive Ion Etch

For the isotropic etching of Si, SF_6/O_2 gases provide a high etch rate and a high degree of selectivity.[29,30] The mix primarily dissociates into SF_5*, F*, O* and low levels of SF_4* radicals. The fluorine atom density increases due to the reaction of O_2 with SF_x* forming SO_2 and SO_4, and the reaction of SF_6 with O* forming SOF_4.[31] The etch rate is initially high because of the higher fluorine atom density and then decreases due to a growing $Si_xO_yF_z$ passivation layer and fluorine atom dilution. We found that a SF_6/O_2 mix of 21/15 achieved a Si:SiO_2 selectivity of 100:1, however as the microdisks became more undercut anisotropic etching became more

Downloaded From: http://proceedings.spiedigitallibrary.org/ on 11/18/2015 Terms of Use: http://spiedigitallibrary.org/ss/TermsOfUse.aspx

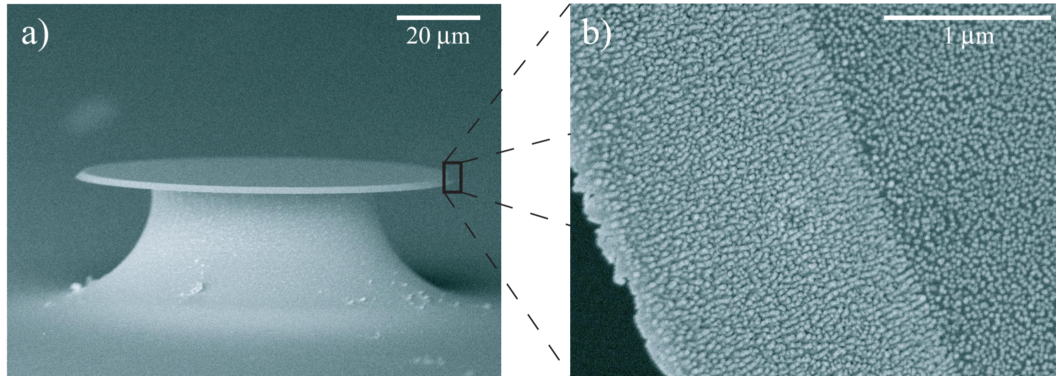

Figure 5. SEM images of a microdisk. (a) A 100 μm diameter silica microdisk. (b) The edge of the microdisk exhibits etch damage from the reactive ion etch.

evident, limiting the rate of undercut, and ultimately limiting the size of the microtoroid in the following reflow process. The mix was adjusted to 21/7 to reduce this problem at the expense of a poorer selectivity of 50:1, at a temperature of 25°C. Both physical and chemical etching processes are present in a reactive ion etch. In chemical etching, the etching process takes place via the chemical reaction of radicals with the substrate; whilst the physical etching mechanism is ion bombardment of the surface of the substrate. Hence, for an isotropic etch, chemical etching must dominate physical etching. This is achieved by changing the bias voltage and the gas pressure. For a low bias voltage there is less physical etching of the wafer from the ion species in the chamber. For a higher pressure the etching species have a shorter mean free path and so the etching is less directional. Pressures of 400 mTorr with a power of 200 W and a bias voltage of -17 V were suitable for our reactor (Oxford Plasmalab 80 Plus). For higher pressures the electrons cannot gather sufficient energy, because of collisions, to overcome the ionization potential of the gas (Paschen's law) and with the subsequent decrease in ionization the etch rate slows. For higher SF_6/O_2 flow rates the average length of time a gas molecule spends in the etching chamber is decreased reducing the build up of chemical etching species and hence the chemical etching rate. The result is a slower more physical (anisotropic) etch. However, a reduced flow rate results in a reduction in radical concentration and a consequential reduction in the total etch rate. For our work we found an SF_6 flow rate of 42 sccm a good compromise. SEM images of a typical microdisk produced using our process are shown in Fig. 5. Both the isotropic nature of the undercut and the $\sim 45^o$ wedge profile due to the wet etch process are clearly evident in Fig. 5(a). Fig. 5(b) shows the damage to the silica microdisk caused by the reactive ion etching process.

4.3. Laser Reflow

There are four significant loss mechanisms for whispering gallery mode resonators: material loss, scattering loss, coupling loss and radiation loss. In our case with 80 μm diameter microtoroids, the radiation loss is insignificant.[22] Absorption losses account for the attenuation of the wave due to the material of the waveguide and scattering losses are due to surface roughness. In order to reduce surface roughness the edge of the microdisk is reflowed with a CO_2 laser,[2,32,22] to leave a surface finish comparable to microtoroids produced by XeF_2 etch(Fig. 6). The thermal conductivity of silicon is on the order of one hundred times greater than that of silica, and unlike silicon, silica also strongly absorbs CO_2 laser radiation. Due to this strong temperature dependence and the thermal isolation of the edge of the microdisk its rim is selectively reflowed leaving the pedestal significantly cooler during the reflow process.[22] In our system the pulse duration, shape and intensity of the CO_2 laser can all be independently controlled. Optimal results were achieved with a 100 ms pulse ramped to an intensity of 1 W with a focal spot of approximately 200 μm. Fig. 6 shows a microtoroid that has been reflowed from a microdisk of the type displayed in Fig. 5(a). The diameter of the microtoroid has decreased to 76 μm and the minor diameter of the rim is 3 μm. Fig. 6(b) clearly shows the improvement in the surface quality, with an observed reduction in surface roughness from ~ 30 nm to ~ 2 nm.

Downloaded From: http://proceedings.spiedigitallibrary.org/ on 11/18/2015 Terms of Use: http://spiedigitallibrary.org/ss/TermsOfUse.aspx

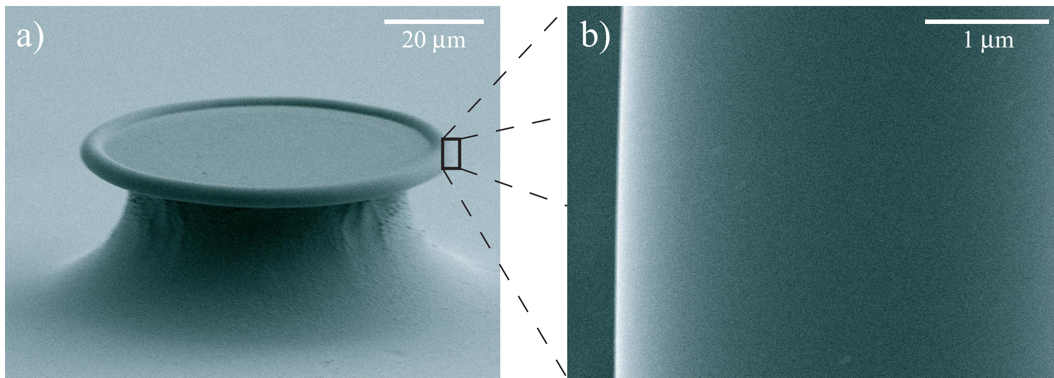

Figure 6. SEM images of a microtoroid. (a) A 100 μm diameter silica microdisk has been reflowed into a $\sim$80 μm microtoroid. (b) Magnified image of the periphery of the microtoroid.

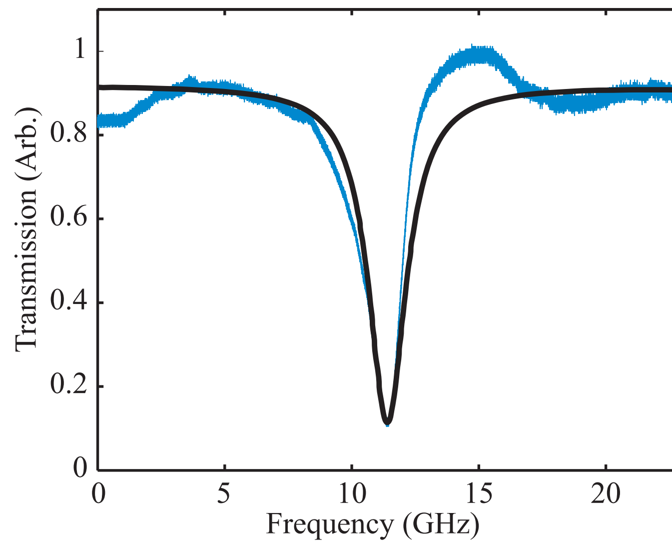

Figure 7. Resonance of a fabricated microtoroid cavity. For $T_{\min} = 0.125$ and $\Delta\omega = 2\pi \times 1.8$ GHz the Lorentzian (dark curve) gives an estimate of the linewidth and a calculated value of the intrinsic Q of 1.6×10^5 that corresponds to a loaded Q of 1.1×10^5.

Downloaded From: http://proceedings.spiedigitallibrary.org/ on 11/18/2015 Terms of Use: http://spiedigitallibrary.org/ss/TermsOfUse.aspx

4.4. Results

Our microresonators were optically excited with 1550 nm light from a New Focus Velocity laser (model 6328). This excitation was achieved using a tapered optical fiber as discussed in Section 2[22] which was fabricated from standard telecom fiber heated with a hydrogen torch and stretched to a diameter of the order of 1 μm. The resonator is positioned relative to the taper using a piezo stage with micrometers for coarse adjustment. Single microtoroid resonances were observed by monitoring the transmitted power through the taper and scanning the laser frequency. Fig. 7 shows a typical resonance and Lorentzian fit with the parameters $T_{\min} = 0.125$, and $\Delta\omega = 2\pi \times 1.8$ GHz, where $T_{\min}$ is the minimum transmission spectral response and $\Delta\omega$ is the FWHM linewidth. This fit gives a loaded quality factor of

$$Q = \frac{\omega}{\Delta\omega} = 1.1 \times 10^5. \tag{17}$$

Eq. (10) can be used to infer the intrinsic quality factor Q_i of the microtoroid from these measurements. For typical microtoroids the backscattering rate b is of the order of 10 MHz.[22] Hence, $b \ll \Delta\omega$ for our resonators, and it is reasonable to simplify Eq. (10) by neglecting b. Since $T_{\min}$ occurs on resonance $\Delta = \omega' = 0$, such that $Z = \kappa$ and

$$T_{\min} = \left[1 - 4\frac{\kappa_i}{\kappa} + 4\frac{\kappa_i^2}{\kappa^2}\right]. \tag{18}$$

From Eq. (1) we see that $\kappa_i/\kappa = Q/Q_i$ so that

$$T_{\min} = \left[1 - 4\frac{Q}{Q_i} + 4\frac{Q^2}{Q_i^2}\right]. \tag{19}$$

Solving this equation for Q_i we find

$$Q_i = \frac{2Q}{1 \pm \sqrt{T_{\min}}}, \tag{20}$$

where the + and - solutions respectively relate to the under- and over-coupled regimes. For our measured values of $T_{\min}$ and Q we find that $Q_i = 1.6 \times 10^5$. A similar calculation applied to a typical microdisk prior to reflow gave the lower value of $Q_i = 1 \times 10^4$. Both results compare favorably to the work of Verbert[28] who observed a Q of 3×10^3 for microdisks produced by a SF_6/O_2 etch. Even with a very high quality surface, the intrinsic Q of our microtoroids is several orders of magnitude lower that the best observed using a XeF_2 etch. It is likely that this is due to absorbtion losses from contaminants introduced in the reactive ion etch that have been reflowed into the rim of the microtoroid. The multitude of reaction mechanisms present in the reactive ion etching process is the likely source of these contaminants.[33] These mechanisms make subtle contributions to the etching process, and any products may condense onto the rim of the microdisks depending on factors such as temperature, pressure and flow rate.

5. CONCLUSION

We have reported on progress towards semiconductor laser frequency stabilization utilising feedback from microtoroidal optical resonators. A simple model of the feedback mechanism was presented, as well as dynamical equations of motion describing the fields within the system. Microtoroids were fabricated with intrinsic quality factors as high as 1.6×10^5. The standard XeF_2 etching stage of the fabrication process was replaced with reactive ion etching. This provides a much improved silicon surface quality, as well as greater controllability of the final physical structure of the resonators. However, the intrinsic quality factor is reduced due to contamination during the reactive ion etching process.

6. ACKNOWLEDGEMENTS

This research was supported by the New Zealand Foundation for Research Science and Technology under the contracts NERF-UOOX0703: Quantum Technologies and NERF-C08X0702: Theory and Applications for Communications Technologies, and by the MacDiarmid Institute for Advanced Materials and Nanotechnology.

Downloaded From: http://proceedings.spiedigitallibrary.org/ on 11/18/2015 Terms of Use: http://spiedigitallibrary.org/ss/TermsOfUse.aspx

REFERENCES

1. K. J. Vahala "Optical microcavities" Nature **424** 839 (2003).
2. D. K. Armani, T. J. Kippenberg, S. M. Spillane and K. J. Vahala "Ultra-high-Q toroid microcavity on a chip" *Nature* **421** 925, (2003).
3. L. Yang, T. Carmon, B. K. Min, S. M. Spillane, and K. J. Vahala, "Erbium-doped and Raman microlasers on a silicon chip fabricated by the sol-gel process", Appl. Phys. Lett., **86** 091114 (2005).
4. A. Polman, B. Min, J. Kalkman, T. J. Kippenberg and K. J. Vahala, "Ultra-low-threshold erbium-implanted toroidal microlaser on silicon", Appl. Phys. Lett. **84** 1037 (2004).
5. T. J. Kippenberg, S. M. Spillane, D. K. Armani, and K. J. Vahala, "Ultralow-threshold microcavity Raman laser on a microelectronic chip", Opt. Lett. **29** 1224 (2004).
6. T. Carmon, H. Rokhsari, L. Yang, T. J. Kippenberg, and K. J. Vahala, "Temporal behavior of radiation-pressure-induced vibrations of an optical microcavity phonon mode", Phys. Rev. Lett. **94** 223902 (2005).
7. T. Aoki, B. Dayan, E. Wilcut, W. P. Bowen, A. S. Parkins, T. J. Kippenberg, K. J. Vahala and H. J. Kimble, "Observation of strong coupling between one atom and a monolithic microresonator" Nature **443** 671 (2006).
8. A. D. Ludlow, M. M. Boyd, T. Zelevinsky, S. M. Foreman, S. Blatt, M. Notcutt, T. Ido, and J. Ye, "Systematic Study of the 87Sr Clock Transition in an Optical Lattice, Phys. Rev. Lett. **96** 033003 (2006).
9. H. Stoehr, F. Mensing, J. Helmcke, and U. Sterr, "Diode laser with a 1 Hz linewidth, Opt. Lett. **31** 736 (2006).
10. F. Schmidt-Kaler, S. Gulde, M. Riebe, T. Deuschle, A. Kreuter, G. Lancaster, C. Becher, J. Eschner, H. Haffner, and R. Blatt, "The coherence of qubits based on single Ca+ ions, J. Phys. B **36** 623 (2003).
11. A. D. Ludlow, X. Huang, M. Notcutt, T. Zanon-Willette, S. M. Foreman, M. M. Boyd, S. Blatt, and J. Ye "Compact, thermal-noise-limited optical cavity for diode laser stabilization at 1×10^{-15}" Opt. Lett. **32** 641 (2007).
12. J. Kitching, R. Boyd and A. Yariv, "Amplitude noise reduction in semiconductor lasers with weak, dispersive optical feedback", *Opt. Lett.* **19** 1331 (1994).
13. G. P. Agrawal and N. K. Dutta, *Long-wavelength semiconductor lasers*, Van Nostrand Reinhold, (1986).
14. A. N. Oraevskii, V. L. Velichansky and A. V. Yarovitsky, "Frequency stabilization of a diode laser by a whispering-gallery mode", Quan. Elec. **31** 897 (2001).
15. M. McGovern *et al.*, in preparation (2007).
16. Roy Lang and Kohroh Kobayashi, "External optical feedback effects on semiconductor injection laser properties", IEEE J. Quan. Elec. **16** 347 (1980).
17. C. Etrich, A. W. McCord and P. Mandel, "Dynamical properties of a laser diode with optical feedback from an external high-finesse resonator", IEEE J. Quan. Elec. **27** 937 (1991).
18. D. R. Hjelme, A. R. Mickelson and R. G. Beausoleil, "Semiconductor laser stabilization by external optical feedback", IEEE J. Quan. Elec. **27** 352 (1991).
19. PH. Laurent, A. Clairon and CH. Breant, "Frequency noise analysis of optically self locked diode lasers", IEEE J. Quan. Elec. **25** 1131 (1989).
20. B. Dahmani, L. Hollberg and R Drullinger, "Frequency stabilization of semiconductor lasers by resonant optical feedback", Opt. Lett. **12** 876 (1987).
21. B. C. Young, F. C. Cruz, W. M. Itano and J. C. Bergquist, "Visible Lasers with Subhertz Linewidths", Phys. Rev. Lett. **82** 3799 (1999).
22. T. J. Kippenberg, "Nonlinear Optics in Ultra-high-Q Whispering-Gallery Optical Microcavities," PhD Thesis, California Institute of Technology, (2004).
23. C. W. Gardiner and M. J. Collett, "Input and output in damped quantum systems: Quantum stochastic differential equations and the master equation", Phys. Rev. A **31** 3761 (1985).
24. V. V. Vassiliev, V. L. Velichansky, V. S. Ilchenko, M. L. Gorodetsky, L. Hollberg, and A. V. Yarovitsky "Narrow-line-width diode laser with a high-Q microsphere resonator" Opt. Comm. **158** 305 (1998).
25. Y. Yamamoto, S. Machida and O. Nilsson, "Amplitude squeezing in a pump-noise-suppressed laser oscillator", Phys. Rev. A **34** 4025 (1986).

Downloaded From: http://proceedings.spiedigitallibrary.org/ on 11/18/2015 Terms of Use: http://spiedigitallibrary.org/ss/TermsOfUse.aspx

26. Marc Madou, *Fundamentals of Microfabrication the Science of Miniaturization*, 2nd Ed, CRC Press, 2002.
27. T. J. Kippenberg, H. Rokhsari, T. Carmon, A. Scherer, and K. J. Vahala, "Analysis of Radiation-Pressure Induced Mechanical Oscillation of an Optical Microcavity," Phys. Rev. Lett., **95**, 033901 (2005).
28. J. Verbert, F. Mazen, T. Charvolin, E. Picard, V. Calvo, P. Noe, J. M. Gerard, and E. Hadji, "Efficient coupling of Er-doped silicon rich oxide to microdisk whispering gallery modes," Appl. Phys. Lett., **86**, 111117 (2005).
29. R. d'Agostino, and D. Flamm, "Plasma etching of Si and SiO_2 in SF_6O_2 mixtures," J. Appl. Phys., **52(1)**, 162 (1981).
30. Tsengyou Syau, B. Jyant Baliga, and Raymond W. Hamaker, "Reactive ion etching of Silicon Trenches Using SF_6/O_2 Gas Mixtures," J. Electrochem. Soc., **138(10)**, 3076 (1991).
31. Henri Jansen, Han Gardeniers, Meint De Boer, Miko Elwenspoek, and Jan Fluitman, "A survey on the reactive ion etching of silicon in microtechnology," J. Micromech. Microeng.**6**, 14 (1996).
32. D. K. Armani, "Ultra-High-Q Planar Microcavities and Appications," PhD thesis, California Institute of Technology, (2005).
33. K. R. Ryan and I. C. Plumb. "A model for the etching of Silicon in SF_6/O_2 plasmas," Plasma Chemistry and Plasma Processing, **10(2)**, 207 (1990).

Downloaded From: http://proceedings.spiedigitallibrary.org/ on 11/18/2015 Terms of Use: http://spiedigitallibrary.org/ss/TermsOfUse.aspx